Structural clustering and functional profiling of NMAN-causing variants in HINT1 suggest personalized therapeutic strategies

Silvia Amor-Barris[1,2#], Tamas Lazar[3,4#], Ayse Candayan[1,2], Luiza L. P. Ramos[1,2], Kristien Peeters[1,2], Shoshana J. Wodak[3] and Albena Jordanova[1,2,5*]

[1] Molecular Neurogenomics Group, VIB Center for Molecular Neurology, VIB, Antwerp, Belgium

[2] Molecular Neurogenomics Group, Department of Biomedical Sciences, University of Antwerp, Belgium

[3] VIB-VUB Center for Structural Biology, Vlaams Instituut voor Biotechnologie (VIB), Brussels, Belgium

[4] Structural Biology Brussels, Department of Bioengineering, Vrije Universiteit Brussel, Brussels, Belgium

[5] Molecular Medicine Center, Department of Medical Chemistry and Biochemistry, Medical University - Sofia, Sofia, Bulgaria

[#] Equally contributing first co-authors

* Corresponding author - email: albena.jordanova@uantwerpen.vib.be

ABSTRACT

Background: Biallelic loss-of-function variants in *HINT1* cause neuromyotonia-associated axonal neuropathy (NMAN). Affected patients present from an early onset with a motor-greater-than-sensory polyneuropathy that is currently incurable. NMAN is a global cause of inherited peripheral neuropathy with higher prevalence in Europe and Asia. Nearly 30 distinct NMAN-associated variants have been reported to date, mostly in sporadic patients and small families. There is limited functional characterization of most of them, resulting in limited knowledge on their pathogenic mode of action and hindering the development of therapeutical strategies.

Methods: We systematically (re-)evaluated the pathogenicity of all reported *HINT1* variants associated with NMAN using several *in silico* pathogenicity predictors used in the standard of care genetic testing. Fifteen missense and one truncating variants were further mapped onto the HINT1 crystal structure and grouped according to their spatial distribution. We combined several structural modeling tools to assess the impact of the variants on protein stability in both monomeric and dimeric forms. These variants underwent further functional validation by immunoblotting in both HeLa *HINT1* knockout cell lines and in a *S. cerevisiae* strain deficient for the HINT1 orthologue. Finally, we tested the *in vivo* functionality of each variant by its ability to rescue yeast growth under stress conditions.

Results: Our combinatorial approach allowed the systematic characterization and (re-)evaluation of all known *HINT1* variants associated with NMAN, enabling improved pathogenicity classification. Additionally, this standardized functional assessment allowed their categorization into four structure-based groups: 1) truncating variants; 2) variants of the catalytic pocket; 3) variants at the dimer interface; 4) variants in the distal β-hairpin and nearby loop. Functional tests in yeast and mammalian disease models demonstrated their detrimental- yet differential -effect on HINT1 function, enabling structure-function correlations.

Conclusions: Our standardized experimental pipeline allows for the characterization of newly discovered HINT1 variants in the context of NMAN, facilitating their pathogenicity interpretation. This work

highlights the value of combining structural and functional approaches to understand better the underlying disease mechanisms. Our findings provide the rational basis for patient stratification and the development of personalized treatment strategies.

Keywords: axonal peripheral neuropathy, variant pathogenicity, protein structure and stability, precision medicine, HINT1, NMAN

76 **INTRODUCTION**

77 The widespread adoption of massive parallel sequencing technologies dramatically increased the number
78 of known disease-causing genes and variants [1-3]. Rare diseases have particularly benefited from this
79 advancement and more than 180 novel disease-causing genes were identified within three years after the
80 commercialization of whole-exome sequencing [3]. While these technological improvements have ended
81 the diagnostic odyssey for many patients, they have yet to translate into widely available therapies. Over
82 6,000 unique rare diseases affecting an estimated 350 million people worldwide have been identified so far,
83 with 80% having a genetic origin. Yet, there is an FDA-approved treatment available for only 5% of
84 them[4]. In rare neuromuscular disorders, most available therapies focus on symptomatic relief or
85 palliation, with no existing disease-modifying therapies or cures. Identifying novel treatment opportunities
86 is challenging due to the poor understanding of underlying disease mechanisms, the small size of patient
87 cohorts, and the limited commercial incentive for companies to invest in the costly development of such
88 therapies [5, 6].

89 These challenges are exemplified in the case of neuromyotonia-associated axonal neuropathy (NMAN
90 [MIM:137200], also known as HINT1 neuropathy). NMAN is an autosomal recessive disorder caused by
91 the loss of functional histidine triad nucleotide-binding protein 1 (HINT1) [7]. Patients display a motor
92 greater than sensory peripheral polyneuropathy with an age of onset mainly within the first decade of life.
93 The disease is characterized by wasting and weakness of the distal limb muscles, sensory loss, and skeletal
94 deformities. This slowly progressive chronic disease is currently incurable. A characteristic feature of
95 HINT1 neuropathy is neuromyotonia, which is present in 70% of the patients, clinically manifests as
96 delayed muscle relaxation after a voluntary contraction, and is caused by the hyperexcitability of the
97 peripheral nerves [7, 8]. NMAN is reported in patients worldwide, yet it has a non-random geographic
98 distribution. The neuropathy is most prevalent in Europe and Asia due to several founder variants
99 (p.Arg37Pro, p.Cys84Arg, p.Gly89Val, p.Arg95Gln, p.Glu100Gly, p.His112Asn) [8]. Among those,

100 p.Arg37Pro shows a high carrier frequency (1:67-1:250) in Central-Eastern Europe, contributing to the
101 significant morbidity of NMAN in this part of the world [7, 9, 10].

102 HINT1 protein is part of the histidine triad (HIT) superfamily characterized by a highly conserved amino
103 acid motif (His-X-Hix-X-His-X-X, where X= hydrophobic amino acid) in the catalytic core near the
104 carboxyl terminus. It forms a homodimer that functions enzymatically as a purine phosphoramidase [11-
105 13] and has also been described as a (de)SUMOylase [14]. *In vitro,* HINT1 hydrolyzes many different
106 substrates, however, the endogenous substrate(s) and the biological relevance of these activities remain
107 unclear. *In vivo*, HINT1 is a transcriptional regulator involved in apoptosis [15, 16], tumor suppression [17,
108 18], and cardiac hypertrophy [19]. In the central nervous system, it affects the endocannabinoid pathway
109 by modulating the NMDAR activity [20-22]. In the peripheral nervous system, where its deficiency causes
110 NMAN, its role remains utterly uncharacterized.

111 Nearly 30 biallelic variants have been causally associated with NMAN, most of which occur in sporadic
112 patients and often in compound heterozygous states. Characterization of their impact on HINT1 activity
113 was done in only a few cases. In this study, we performed a systematic structural and experimental (re-)
114 evaluation of the impact of 16 selected NMAN-associated variants on HINT1 function, adding novel
115 evidence for their pathogenicity. Importantly, we were able to group the variants based on their differential
116 effect on the HINT1 protein structure and function. Our findings provide novel insights into the
117 pathomechanisms behind NMAN, justifying the implementation of patient stratification strategies and the
118 development of personalized treatment options.

119

120 **MATERIAL AND METHODS**

121 ***Selection of HINT1 variants***

122 We conducted a comprehensive literature search using PubMed to identify HINT1 variants associated with
123 NMAN that have been reported in peer-reviewed articles published between 2012 and 2024. For each
124 reported variant, we determined allele frequency using data from the Genome Aggregation Database

125 (gnomAD v4.1). Subsequently, we performed *in silico* analyses using pathogenicity predictions tools
126 routinely employed in diagnostic settings, including CADD (v3) [23], REVEL (v4) [24], AlphaMissense
127 [25], and SpliceAI [26].

128 ***Solvent accessible surface area and in silico protein fold stability calculations***

129 The effect of the missense variant on the protein stability was calculated using FoldX-4 [27], SDM [28],
130 mCSM [29], DUET [30], ENCoM [31], and DynaMut [32]. These methods combine information from
131 protein sequences, 3D structures, and crude physicochemical parameters to calculate the change in protein
132 folding free energy (stability) ($\Delta\Delta G$). The calculations were carried out on the isolated HINT wild-type
133 monomer and on the homodimer to evaluate separately the effect of the variants on the stability of individual
134 subunits and the dimer.

135 We calculated the solvent-accessible surface area of individual residues (ASA_R) in the monomer and the
136 dimer. Based on these, we calculated the buried surface area of a residue (BSA_R) upon dimer formation
137 representing the contribution of the residue to the dimer stability [33]; which fraction gets buried in the
138 dimer ($fBSA_R = BSA_R / ASA_R(monomer)$), and the residue relative accessible surface area $RSA_R = [ASA_R$
139 $(monomer\ or\ dimer) / ASA_R(Gly\text{-}X\text{-}Gly)]$, where 'x' represents the same residue in the free dipeptide unit.
140 The ASA_R of the residue in the 'x' position of this very flexible dipeptide is taken to represent its ASA in
141 the unfolded state of the protein. The various solvent-accessible surface area calculations were performed
142 with the software FreeSASA 2.0.3[34] using default parameters.

143 ***Cloning and creation of HINT1 expression plasmids***

144 Yeast and mammalian expression plasmids with human *HINT1* were generated in previous studies[7, 35].
145 *HINT1* variants were introduced with site-directed mutagenesis using the KAPA HiFi kit (Roche
146 Diagnostics, Basel, CH). Verification of the variants was done using Sanger sequencing.

147 ***Cell line establishment and culture***

148 *HINT1* HeLa KO cell lines were created using CRISPR/Cas9, as described previously[35]. HeLa cells were
149 maintained in high-glucose DMEM (Gibco, Waltham, MA, USA) supplemented with 10% heat-inactivated

150 fetal bovine serum (FBS, Gibco, Waltham, MA, USA), 1% penicillin/streptomycin (Gibco, Waltham, MA,
151 USA), and 1% glutamine (Gibco, Waltham, MA, USA). Cells were grown at 37ºC and 5% CO_2 in a
152 humidified atmosphere.

153 ***Cell transfection***

154 HeLa cells were transiently transfected using polyethylenimine (PEI) MW25000 (Polysciences,
155 Warrington, PA, USA) with a pCAGGAS vector carrying human WT or variant HINT1. A pCAGGS-MBP
156 was used as an empty vector control. Cells were seeded in a 6-well plate the day before the transfection in
157 a complete medium without antibiotics. Cells were transfected with PEI and 250ng plasmid when 70-80%
158 confluency was reached.

159 ***Immunoblotting***

160 Cells were lysed in RIPA lysis buffer (20 mM Tris-HCl pH=7.4; 150 mM NaCl; 0.1% Nonidet P-40; 0.5%
161 sodium deoxycholate; 0.1% sodium dodecyl sulfate) supplemented with Halt™ Protease Inhibitor Cocktail
162 (ThermoFisher Scientific, Waltham, MA, USA) for 30 min on ice and cleared by centrifugation for 10 min
163 at 14000 RPM. Protein concentration was measured with the Pierce BCA protein assay kit (ThermoFisher
164 Scientific, Waltham, MA, USA) and adjusted to 20µg per sample. Lysates were boiled for five min at 95ºC
165 in reducing Laemmli sample buffer (Bio-Rad, Hercules, CA, USA) supplemented with 100mM 1.4-
166 Dithiothreitol (DTT).

167 Yeast proteins were extracted following a previously published protocol[35]. Briefly, yeast cells were
168 collected before the stationary phase (OD_{600nm}=1) by centrifugation. Then, cells were washed first with
169 2.0M LiAc and then 0.4M NaOH for 5 min on ice. Cells were finally boiled for five min at 95ºC in Laemmli
170 sample buffer (Bio-Rad, Hercules, CA, USA) supplemented with 100mM DTT.

171 Proteins were separated in 4-15% Mini-PROTEAN® TGX Stain Free™ Protein gels (Bio-Rad, Hercules,
172 CA, USA) and transferred to a nitrocellulose membrane (Hybond™-P, GE Healthcare, Chicago, IL, USA)
173 using the semi-dry Trans-Blot® Turbo™ Transfer System (Bio-Rad, Hercules, CA, USA). Membranes were
174 blocked for an hour at room temperature with 5% milk powder diluted in PBS supplemented with 0.1%

175 Tween-20 and then incubated with a primary antibody overnight at 4ºC and one hour with a secondary
176 horseradish peroxidase-conjugated antibody at room temperature. Membranes were developed with
177 Enhanced Chemiluminescence ECL Plus™ (ThermoFisher Scientific, Waltham, MA, USA) and imaged
178 with ImageQuant™ LAS 4000 (GE Healthcare, Chicago, IL, USA). The antibodies used in this study were
179 polyclonal rabbit anti-human HINT1 antibody (1:1000, Sigma, San Luis, MO, USA), and to demonstrate
180 equal loading mouse monoclonal anti-β-actin antibody (1:5000, Sigma, San Luis, MO, USA), mouse
181 polyclonal anti-α-tubulin antibody (1:5000, Abcam, Cambridge, UK) or mouse polyclonal anti-PKG
182 antibody (1:10.000, Sigma, San Luis, MO, USA).

183 ***Dimerization reaction***

184 Cells were harvested and lysed in 0.2 triethanolamine, pH=8.0, with 0.3 mg/ml of dimethyl adipimidate
185 (DMP, ThermoFisher Scientific, Waltham, MA, USA) for 1 hour with vertical mixing. The lysates were
186 cleared, and protein concentration was measured before immunoblotting.

187 ***Yeast strain and transformation***

188 *S. cerevisiae* strain BY8-5c (MATα *ura3-52 his3Δ200 trp1Δ901 lys2-801 suc2-Δ9 leu2-3,112*
189 *hnt1Δ::URA3*)[11] was kindly provided by Dr. Brenner, University of Iowa, USA. Yeast cells were cultured
190 in rich (YP) medium supplemented with 2% glucose. The transformation of BY8-5c with the pAG415GPD
191 expression plasmids carrying WT or variant *HINT1* was done using the LiAc/SS carrier DNA/PEG
192 method[36]. Positive clones were selected in minimal medium without Leucine (SD-Leu) supplemented
193 with 2% glucose.

194 ***Spot assay***

195 Pre-cultures of the different yeast clones were grown overnight in SD-Leu supplemented with glucose.
196 Absorbance was measured and adjusted to an optical density of OD_{600nm}=1. Serial dilutions of each culture
197 were performed, and 5µl culture was spotted on SD-Leu agar plates supplemented with either 2% glucose
198 or 2% galactose. Plates were incubated for three days at 39ºC.

199

200 **RESULTS**

201 ***Systematic evaluation of NMAN-associated variants using pathogenicity predictors defines their***
202 ***pathogenic character***

203 To select HINT1 variants to be investigated in this study, we curated articles published between 2012 and
204 2025 that reported genetic alterations of HINT1 in patients with peripheral neuropathies. A total of 29
205 *HINT1* variants were retrieved (Table 1), including 21 missense, five stop-gain (p.Gln9Ter, p.Ser61Ter,
206 p.Gln62Ter, p.Gln106Ter, p.Trp123Ter) [7, 9, 37, 38], two small exonic deletions (p.Phe33Leufs*22,
207 p.His51Phefs*18) [39, 40], one deletion affecting the splice-donor site of the canonical transcript (c.112-
208 1delG)[41], and one complex chromosomal rearrangement causing start-loss (g.
209 [131164372_131165305delins131165015_131165143inv; 131165362_131165385del]) [42]. In most of the
210 patients, the age of onset of the neuropathy was in the first decade of life, even though cases with later onset
211 (early 30s) have also been reported. Neuromyotonia, the hallmark sign of the disease, was reported in 73%
212 of the affected individuals.

213 Overall, 12 out of 29 variants (41%) were recurrent and have been identified in more than two unrelated
214 patients in either compound heterozygous or homozygous state. Among them, there were seven founder
215 variants in Europe (p.Arg37Pro, p.Cys84Arg, p.Gly89Val, p.Arg95Gln, p.Glu100Gly, and p.His112Asn)
216 [8, 35, 43] and Asia (p.Cys38Arg) [24]. Notably, the p.Arg37Pro allele was present in nearly 80% of all
217 NMAN patients. The 17 remaining variants were identified in sporadic cases only: five were homozygous
218 in non-consanguineous families, and 11 were in a compound heterozygous state (Table 1).

219 Most of the variants had a very low allele frequency (<0.0005%) across all represented genetic ancestries
220 (gnomAD v 4.1), and a substantial fraction (15/28) was absent from population databases. According to *in*
221 *silico* predictors of variant pathogenicity (including CADD [44], REVEL [24], and AlphaMissense [45]),
222 25/29 of the missense variants had a damaging effect. For p.Phe33Ser, p.Glu34Lys, p.Arg37Pro,
223 p.Glu100Gly, there were conflicting results across the three predictors. We categorized all *HINT1* variants
224 according to the American College of Medical Genetics and Genomics (ACMG) guidelines. One variant

225 was classified with unknown significance (VUS) (p.Glu34Lys), thirteen were likely pathogenic, and seven
226 were pathogenic. Two variants with conflicting *in silico* prediction scores (p.Arg37Pro and p.Glu100Gly)
227 were classified as pathogenic by the ACMG guidelines based on the functional data available (PS3).

228 **Table 1: Summarized overview of variants identified in NMAN patients.**

Variant	Zygosity	Number of families	gnomAD (v4.1) AF	CADD (v3)	REVEL (v4)	AlphaMissense	SpliceAI	ACMG criteria	ACMG classification	First described in
NM_005340.7:c.25C>T (p.Gln9Ter)	Hm	1	0.000006212	44	NA	NA	0	PM2, PM3, PVS1 PP2, PP4	Pathogenic	[38]
NM_005340.7:c.98T>C (p.Phe33Ser)	CH	1	0.000004957	26.7	0.615	0.738	0.01	PM2, PM3, PP2, PP4	Likely Pathogenic	[46]
NM_005340.7:c.99del p.Phe33Leufs*22	Hm	1	Absent	NA	NA	NA	0.02	PM2, PM3, PVS1, PP2, PP4	Pathogenic	[40]
NM_005340.7:c.100G>A (p.Glu34Lys)	Hm	1	Absent	25.5	0.735	0.746	0.03	PM2, PP2, PP3, PP4	VUS	[47]
NM_005340.7:c.100G>C (p.Arg37Pro)	CH/Hm	144	0.0002219	6.61	0.56	0.898	0.02	PS3, PM2, PM3, PP1, PP2, PP4	Pathogenic	[7]
NM_005340.7:c.112T>C (p.Cys38Arg)	CH/Hm	5	0.000001268	32	0.906	0.993	0	PM2, PM3, PP2, PP3, PP4	Likely Pathogenic	[46]
NM_005340.7: c.112-1delG	CH	1	Absent	34	NA	NA	1	PM2, PM3, PVS1 PP2, PP4	Pathogenic	[41]
NM_005340.7:c.145C>T (p.Pro49Ser)	CH	1	Absent	28.1	0.878	0.757	0	PM2, PM3, PP2, PP3, PP4	Likely Pathogenic	[48]
NM_005340.7:c.152A>G (p.His51Arg)	CH	1	0.00000186	25.9	0.932	0.982	0	PS3, PM2, PP2, PP3, PP4	Pathogenic	[7]
NM_005340.7:c.148_149delAC (p.His51Phefs*18)	Hm	1	Absent	NA	NA	NA	0	PM2, PM3, PVS1 PP2, PP4	Pathogenic	[39]
NM_005340.7:c.171G>C (p.Lys57Asn)	CH	1	Absent	25.4	0.745	0.971	0.02	PM2, PM3, PP2, PP3, PP4	Likely Pathogenic	[46]
NM_005340.7:c.180_181delAT (p.Ser61Profs*8)	Hm	1	Absent	NA	NA	NA	0.02	PM2, PM3, PVS1 PP2, PP4	Pathogenic	[37]
NM_005340.7:c.182C>T (p.Gln62Ter)	CH	1	0.00000062	42	NA	NA	0	PM2, PM3, PVS1 PP2, PP4	Pathogenic	[7]

NM_005340.7:c.188T>A (p.Ile63Asn)	CH/Hm	2	0.00000186	27.9	0.807	0.896	0	PM2, PM3 PP2, PP3, PP4	Likely Pathogenic	[49]
NM_005340.7:c.205T>C (p.Cys84Arg)	CH/Hm	6	0.000003719	27.9	0.937	0.889	0	PS3, PM2, PM3,PP2, PP3, PP4	Pathogenic	[7]
NM_005340.7:c.266G>T (p.Gly89Val)	CH/Hm	4	0.00000062	25.1	0.861	0.633	0	PM2, PM3, PP2, PP3	Likely Pathogenic	[7]
NM_005340.7:c.278G>A (p.Gly93Asp)	CH/Hm	3	0.000006817	25.7	0.907	0.976	0	PS3, PM2, PM3, PP2, PP3, PP4	Pathogenic	[7]
NM_005340.7:c.278G>T (p.Gly93Val)	Hm	1	Absent	25.7	0.906	0.966	0	PM2, PM5, PP2, PP3, PP4	Likely Pathogenic	[50]
NM_005340.7:c.281A>G (p.Tyr94Cys)	CH	1	Absent	25.9	0.888	0.741	0	PM2, PM3, PP2, PP3	Likely Pathogenic	[41]
NM_005340.7:c.284G>A (p.Arg95Gln)	CH	2	0.00002975	25.3	0.854	0.899	0	PS3, PM2, PM3, PP2, PP3	Pathogenic	[35]
NM_005340.7:c.281A>G (p.Val97Met)	Hm	2	Absent	26.9	0.830	0.911	0.01	PM2, PM3, PP2, PP3, PP4	Likely Pathogenic	[51]
NM_005340.7:c.299A>G (p.Glu100Gly)	CH/Hm	4	0.000001859	25	0.471	0.741	0	PS3, PM2, PP2	Pathogenic	[43]
NM_005340.7:c.311G>T (p.Gly104Arg)	Hm	1	0.000003718	28,8	0,936	0,974	0	PM2, PP2, PP3	Likely pathogenic	[52]
NM_005340.7:c.316C>T (p.Gln106Ter)	CH	3	0.000004338	40	NA	NA	0	PS3, PM2, PM3, PP2, PP3	Pathogenic	[9]
NM_005340.7:c.334C>A (p.His112Asn)	CH/Hm	12	0.00002108	28	0.901	0.984	0	PS3, PM2, PM3, PP2, PP3, PP4	Pathogenic	[7]
NM_005340.7:c.341A>G (p.His114Arg)	CH	1	Absent	26.1	0.989	0.983	0.01	PM2, PP2, PP3	Likely Pathogenic	[53]
NM_005340.7:c.355C>T (p.Arg119Trp)	CH/Hm	3	0.000009925	25.9	0.703	0.919	0.08	PM2, PP2, PP3	Likely Pathogenic	[54]
NM_005340.7:c.356G>T (p.Arg119Leu)	Hm	1	Absent	26	0.814	0.902	0.01	PM2, PP2, PP3	Likely Pathogenic	[55]
NM_005340.7:c.356G>T (p.Trp123X)	Hm	2	Absent	38	NA	NA	0.04	PS3, PM2, PP2, PP3	Pathogenic	[7]

229 CH: compound heterozygous, Hm: homozygous, AF: allele frequency.

230 ***ClinVar reported variants of uncertain significance in HINT1 highlight the need for re-assessment of***
231 ***pathogenicity***

232 ClinVar is a public archive for human variation reporting variants found in patient samples, pathogenicity
233 classifications, drug responses, submitter information, and additional supporting data. As such, it is a freely
234 accessible resource for curating both published and unpublished data on variants observed in patients and
235 has long been used for variant interpretation. A total of 121 HINT1 variants (excluding copy number
236 variants impacting HINT1 together with multiple other genes) have been submitted to the ClinVar database
237 to date (Additional File 1). Approximately 21.5% of them (26/121) have a germline classification of
238 pathogenic or likely pathogenic. Two percent of the ClinVar variants (3/121) have conflicting
239 interpretations of pathogenicity, and interestingly, these were all previously reported in NMAN cases
240 (p.Ile63Asn, p.Arg95Gln, p.Arg119Trp). The remaining 38% of the variants (43/121) are classified as
241 benign or likely benign. Additionally, 40% of the ClinVar variants (49/121) were reported to have uncertain
242 significance, including three variants identified in NMAN patients (p.Tyr94Cys, p.Glu100Gly,
243 p.His114Arg).

244 Using AlphaMissense, we calculated pathogenicity scores for all possible amino acid substitutions of each
245 residue across the HINT1 sequence. By visualizing these scores in a heatmap, we identified regions that are
246 either more tolerant to missense variants or serve as "hotspots" for substitutions with a deleterious
247 effect(Fig. 1). We then integrated this data with the positions of reported NMAN-associated variants and
248 those extracted from the ClinVar database. Our analysis revealed that most of the 21 missense variants
249 analyzed in this study cluster within regions with high pathogenicity scores. Notably, the distribution of
250 ClinVar variants with uncertain significance along the protein sequence differed significantly from that of
251 the NMAN-associated variants (Fig. 1B), and they showed lower mean pathogenicity scores (Fig. 1C). This
252 suggests that many VUS reported in the ClinVar database are likely benign, however experimental
253 validation is necessary to clarify their true clinical significance.

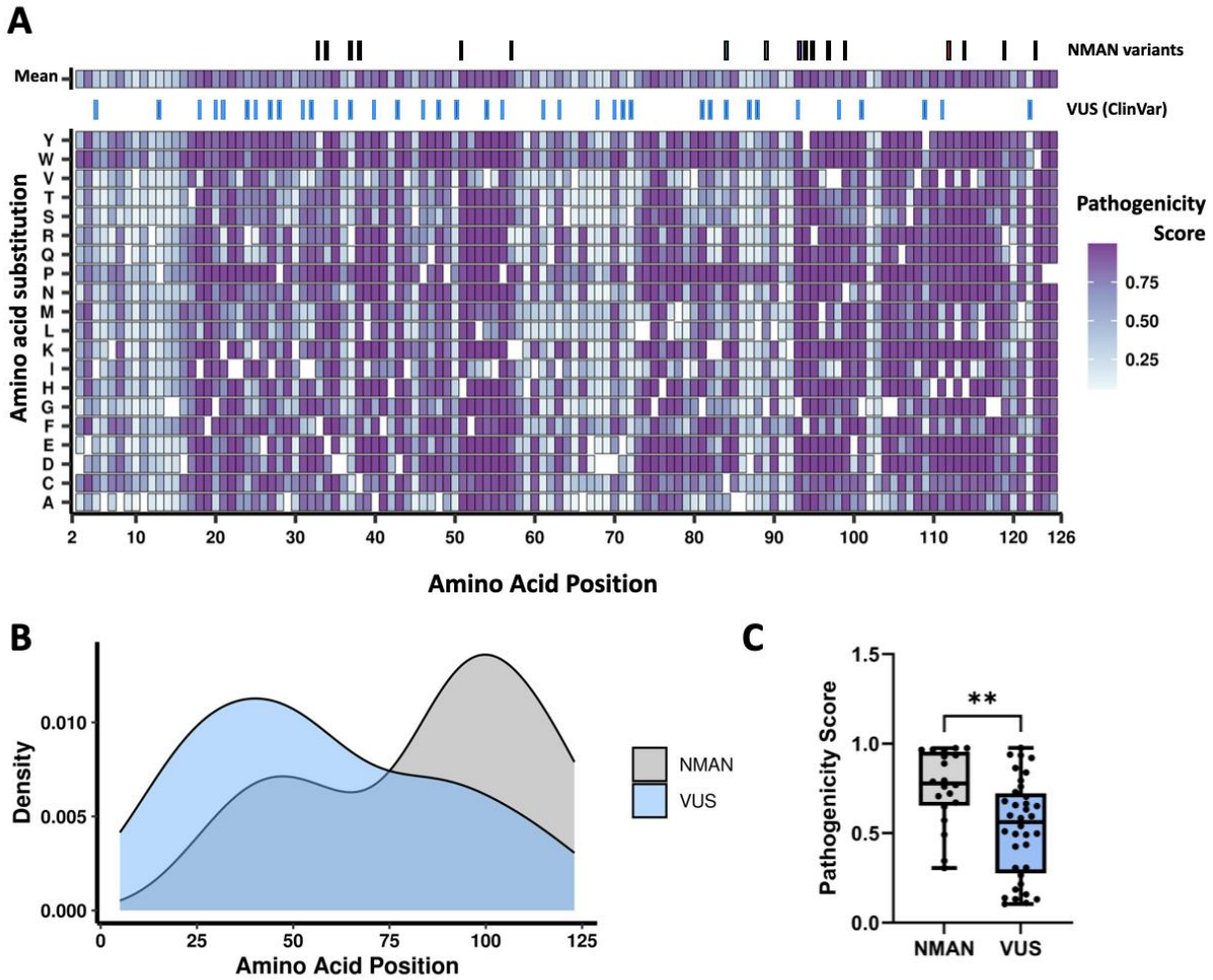

Figure 1. **Pathogenicity scores for missense mutations across HINT1 primary structure calculated by AlphaMissense. A)** Heat map representing every position in the HINT1 amino acid sequence and the pathogenicity score calculated by AlphaMissense of every possible amino acid substitution. Synonymous variants are depicted as white spaces. On top, the average pathogenicity score for each amino acid in the HINT1 sequence. Blue rectangles indicate the positions of the variants of uncertain significance (VUS) submitted to ClinVar. Black rectangles indicate the position of the variants reported in NMAN patients characterized in this study. **B)** Kernel density estimates were plotted to compare the distribution of the VUS reported in ClinVar (blue) and the NMAN-associated variants (grey). Wilcoxon Rank-sum test showed significant differences between the two distributions (p=0.004288). **C)** Comparison of the predicted pathogenicity score by AlphaMissense shows a significantly lower pathogenicity score (unpaired t-test, p=0.0016) for the VUS reported in ClinVar compared to the NMAN-associated variants

265

266 ***A combination of computational approaches and 3D mapping of NMAN causal variants identifies***
267 ***structural clusters***

268 To study the effect of each NMAN-associated variant on the HINT1 protein, we used a combinatorial
269 computational approach where we assessed the impact of residue positions, solvent-accessible surface
270 areas, protein stability, and conservation. Together, these allowed us to identify four (non-mutually
271 exclusive) groups in which the variants showed commonalities. The first group contained all predicted loss-
272 of-function (pLoF) genetic variants. These include four stop-gain variants (p.Gln9Ter, p.Ser61Ter,
273 p.Gln62Ter, p.Gln106Ter), two small exonic deletions (p.Phe33Leufs*22, p.His51Phefs*18), the loss of
274 splice donor-site of the canonical transcript (c.112-1delG), and the start-loss caused by a complex
275 chromosomal rearrangement (g.
276 [131164372_131165305delins131165015_131165143inv;131165362_131165385del]). In all cases, these
277 variants either resulted in a truncated polypeptide lacking the characteristic HIT motif, potentially triggering
278 nonsense-mediated mRNA decay, or prevented protein production due to start-loss. Therefore, they all lead
279 to non-functional proteins and, hence, are classified as pathogenic (Fig. 2A, black). The remaining genetic
280 variants were classified into three additional structural clusters based on their spatial distribution on the 3D
281 protein structure and the kind of potential change they might impart on the protein. These include a) the
282 catalytic pocket, b) the dimer interface, and c) the distal β-hairpin and nearby loop (Fig. 2A, B).

283 The catalytic pocket cluster (Fig. 2A, B, red) includes all residues directly involved in the phosphoramidase
284 activity of HINT1. These residues are either part of the highly conserved HIT motif (p.His112, p.His114),
285 they help stabilize the product intermediates (p.His51), or contribute to substrate recognition (p.Trp123).
286 Additionally, two residues (p.His114, p.Trp123) contribute to the formation of the dimeric holoenzyme.
287 The high conservation of the affected residues across species highlights their essential function and suggests
288 that their substitution will have a detrimental effect on the enzymatic activity (Additional File 2).

289 Accordingly, all residue substitutions are predicted to destabilize both the monomeric and dimeric forms of
290 HINT1 equally (Fig. 2C).

291 Many residues hit by NMAN missense substitutions (p.Gly89, p.Gly93, p.Tyr94, p.Arg95, p.Val97) cluster
292 at the dimer interface in an antiparallel β-sheet (Fig. 2A, B, purple). Additionally, the p.Arg119 residue,
293 although it does not reside at the dimer interface, forms hydrogen bonds with the C-terminus of the
294 neighboring monomer, further stabilizing the contacts between the two monomers. The majority of the
295 surface area of the residues in this cluster is buried upon formation of the HINT1 wild-type (hWT) dimer
296 (*see Methods for details*), and significantly more than any of the other variants analyzed (BSA_R in
297 Additional File 3), confirming their essential contribution to the stability of the dimer interface. Their
298 substitution with polar or bulkier residues is expected to disrupt the dimer interface, thereby destabilizing
299 the protein. This destabilization is predicted to be higher for the dimeric form compared to the monomeric
300 form, reinforcing their role in dimer formation (Fig. 2C). The residues of this cluster are conserved across
301 species, with the highest conservation seen for p.Tyr94 and p.Arg119 (Additional File 2).

302 The third cluster includes variants affecting residues lying far from the dimer interface and the catalytic
303 pocket. They are located at the surface of the protein, featuring the smallest fraction of buried surface area,
304 and hence remain essentially accessible to solvent in both the monomeric and dimeric forms (Additional
305 File 3). Four residues (p.Phe33, p.Glu34, p.Arg37, p.Cys38) are positioned in a β-hairpin at the N-terminus.
306 The p.Lys57 residue is adjacent to the β-hairpin, and the p.Cys84 is in an α-helix that packs against the β-
307 sheet formed by the hairpin. This cluster contributes to preserving the native helix-sheet interactions (Fig.
308 2, green). Interestingly, this part of the protein exhibits the lowest degree of homology among species, with
309 significant conservation observed only across mammals (Additional File 2). The p.Phe33Ser, p.Glu34Lys,
310 p.Arg37Pro, p.Lys57Asn, and p.Cys84Arg variants of the β-hairpin cluster are predicted to have only mild
311 destabilizing effects on the dimer and monomer, while a higher destabilizing effect is predicted for the
312 p.Cys38Arg variant (Fig. 2C).

313

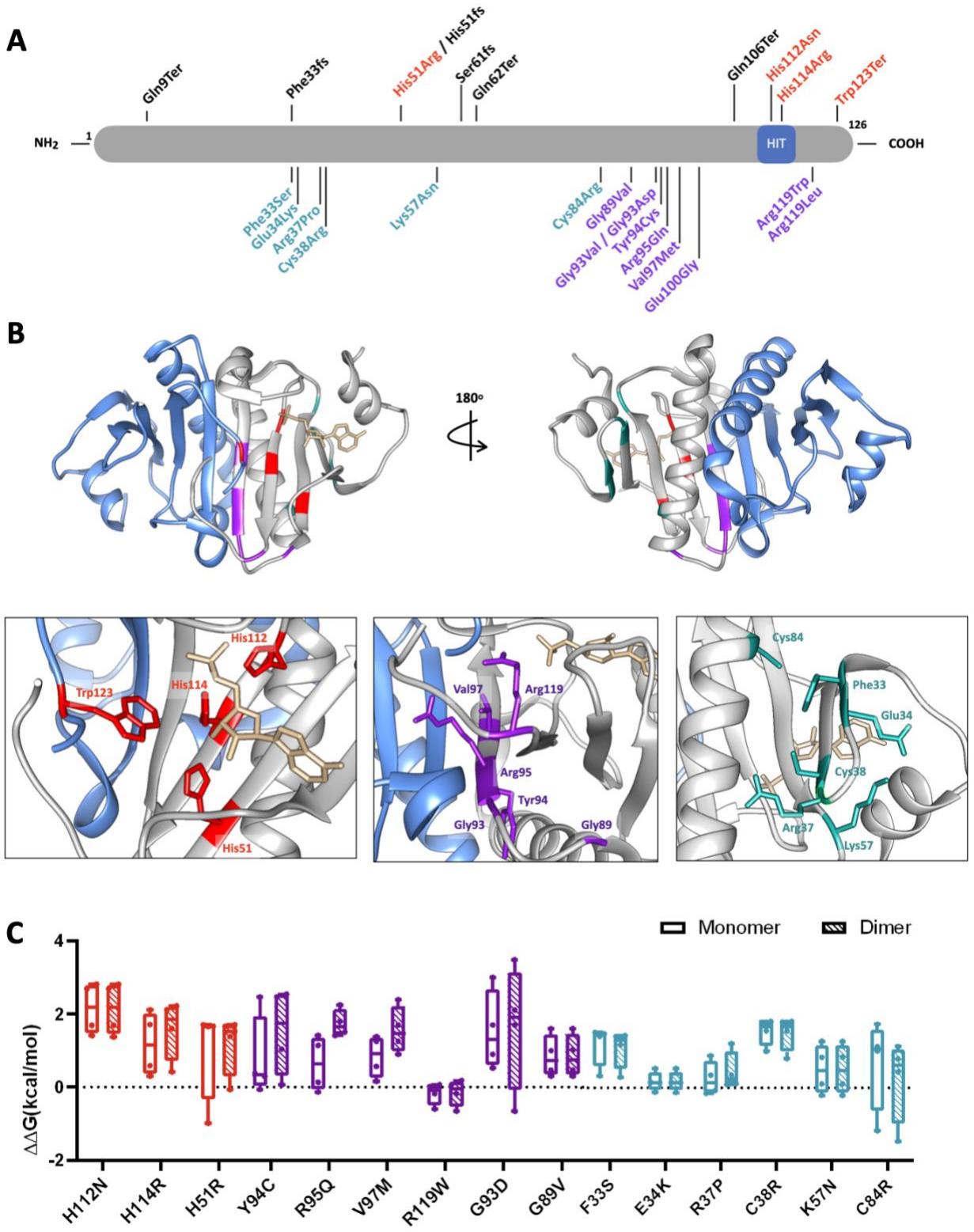

Figure 2. Classification of HINT1 missense variants in structural clusters. **A)** Mapping of the HINT1 missense variants onto the HINT1 protein sequence. The highly conserved HIT motif is represented as a blue box. **B)** Mapping

317 of the residues affected by NMAN-causal variants in the crystal structure of the HINT1 dimer (PDB: 5KLZ). Each
318 monomer is shown in "cartoon" representations and in different colors (blue and silver); AMP is indicated in gold
319 using a "sticks" representation in the catalytic pocket of the enzyme. Close-ups of the three structural clusters
320 identified are shown on the bottom panel. The variants are colored according to the cluster classification. Red: variants
321 at the catalytic site. Purple: variants at the dimer interface. Green: variants in the distal β-hairpin and the hairpin-helix
322 region. **C)** Predicted destabilization effects of the NMAN missense variants on the HINT1 dimer and monomer
323 stability, respectively. PDB structure 5KLZ chain A+B was used as input for evaluating the effects on dimer stability,
324 and chain B alone for monomer stability. The ΔΔG distributions represent the ΔΔG values obtained using the different
325 stability predictors (*see Materials & Methods for details*). Values calculated by FoldX showed the most significant
326 fluctuations, often differing from those of other methods, and were therefore excluded from the plot (for ΔΔG values
327 computed by all methods, see Additional File 3). Because p.Trp123Ter is not a missense variant, the destabilizing
328 effect of early termination of the protein sequence could not be calculated by the stability predictors.

329

330 ***Experimental characterization using functional assays reveals commonalities among variants within the***
331 ***same structural cluster***

332 To functionally assess the impact of the missense variants on the HINT1 structure, we transiently
333 overexpressed the disease-causing alleles in a *HINT1* knock-out (KO) HeLa cell line[35] and quantified the
334 resulting exogenous HINT1 protein abundance by immunoblotting (Fig. 2A). We modeled the most
335 recurrent substitutions for p.Gly93 and p.Arg119 (p.Gly93Asp and p.Arg119Arg) even though other
336 alterations of the same residues are also reported (p.Gly93Val and p.Arg119Leu). When disease-causing
337 alleles impacting the catalytic pocket were transiently expressed in HeLa cells, no HINT1 protein was
338 detected by immunoblotting. The p.His112Asn allele was a notable exception to this, with the resulting
339 HINT1 protein expressed at comparable levels to the endogenous WT protein (Fig. 3A). Our finding aligns
340 well with previous reports showing similar stability and structure of this variant compared to the hWT
341 protein. The six substitutions of the dimer interface cluster had different impacts on the overall stability of
342 the protein in HeLa cells (Fig. 3A). Two of them (p.Val97Met, p.Arg119Trp) heavily impacted HINT1

343 stability, and the resulting proteins could not be detected. Two others (p.Gly93Asp, p.Arg95Gln) caused
344 only a reduction in protein expression levels, whereas the last two variants (p.Gly89Val and p.Tyr94Cys)
345 resulted in proteins expressed at levels similar to that of the hWT protein. Lastly, the β-hairpin cluster
346 variants resulted in proteins with high instability. Only the p.Phe33Ser allele was expressed at similar levels
347 as the hWT protein, whereas only faint traces of the p.Lys57Asn and p.Cys84Arg proteins were detectable
348 by immunoblotting (Fig. 3A).

349 Since HINT1 enzymatic function relies on the correct formation of HINT1 homodimers, we investigated if
350 HINT1 dimerization was impaired in those alleles that did not cause protein instability in our previous
351 analyses. To this end, we treated the cell lysates with dimethyl pimelimidate (DMP), a cross-linking reagent
352 active towards primary amines. DMP has a short linker (7 Å), allowing the study of protein quaternary
353 structures by covalently binding the different subunits together. Protein levels of the monomeric and the
354 dimeric forms of HINT1 were detected via immunoblotting (Fig. 3B), and the ability to form dimers was
355 quantified as a ratio of HINT1 dimer over the HINT1 monomer normalized to the HINT1-hWT
356 overexpression ratio. In cells expressing hWT proteins, two bands were detected, one at 14 kDa (monomer)
357 and another at 28 kDa (dimer). The tested altered proteins showed a heterogenous effect on dimer formation
358 efficiency (Fig. 3B). Only the p.Gly93Asp protein remained monomeric and showed severe dimerization
359 impairment. The remaining proteins were able to form HINT1 dimers, similar to the hWT protein; however,
360 they showed additional features. The p.Phe33Ser showed a slight shift in the molecular weight of the dimer.
361 An even larger shift was observed for the p.His112Asn protein, suggesting the likely presence of an
362 additional binding partner. The p.Tyr94Cys protein size-separated into several bands, indicating that it is
363 prone to aggregation or interacts with another partner(s). Finally, only the p.Gly89Val protein could form
364 dimers as the hWT protein.

365

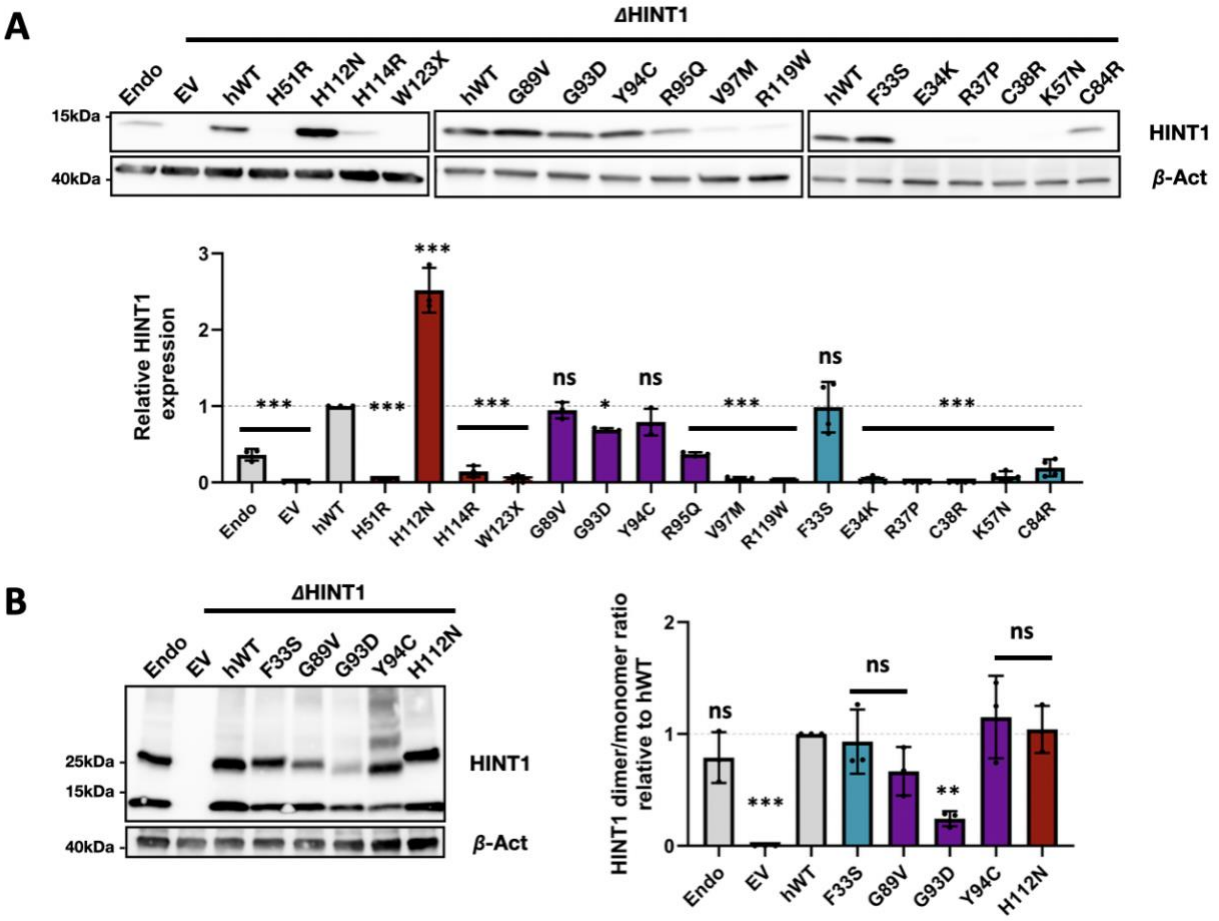

366

367 ***Figure 3: In cellulo characterization of NMAN-associated missense variants in HINT1.*** **(A)** Expression constructs
368 carrying an NMAN allele were transiently expressed in HeLa *HINT1* KO cells, and the HINT1 protein levels were
369 assessed by semiquantitative immunoblotting. Equal loading was validated with β-actin, and relative HINT1
370 expression was normalized to hWT expression. The graph represents the relative quantification of band intensities for
371 three independent replicates. **(B)** Immunoblotting after dimerization reaction using DMP. HINT1 protein expression
372 levels in monomeric (14 kDa) and dimeric (28 kDa) forms could be detected. The level of dimer formation was
373 quantified relative to the monomer expression and normalized to the hWT. One-way ANOVA with Dunnet multiple
374 comparison tests was used in all western-blot quantifications. Bar charts are presented as means with standard error
375 of the mean (s.e.m). ns = no significant, *p<0.05, **p<0.01, *** p<0.001

376

377 Currently, the only *in vivo* model for HINT1 neuropathy uses a yeast strain deficient for *HNT1* (HINT1
378 orthologue). This strain exhibits a growth deficit under restrictive conditions (Galactose, 39°C) that can be
379 complemented by the human HINT1 wild-type protein (hWT), thus providing an easy readout for testing
380 HINT1 functionality[7]. We used this model to assess the detrimental effect of the HINT1 missense variants
381 by first checking the stability of the proteins in the yeast by immunoblotting, followed by testing their
382 functionality based on their ability to rescue the yeast growth deficit.

383 All altered proteins from the catalytic cluster were stably expressed in yeast with only p.His51Arg and, to
384 a lesser extent, p.Trp123Ter, showing relatively lower expression levels (Fig. 4A). Despite their presence,
385 none of them could rescue the growth deficiency, suggesting a loss of catalytic function (Fig. 4B). The
386 proteins harboring variants at dimer interface were all expressed at similar levels to the WT protein, except
387 for p.Val97Met, whose expression was slightly reduced (Fig. 4A). Despite all the corresponding proteins
388 being stably expressed in yeast, only p.Gly89Val caused a complete rescue of the HINT1 growth phenotype,
389 whereas p.Tyr94Cys and p.Arg119Trp enabled only partial recovery of the yeast growth under stress
390 conditions. The remaining three substitutions (p.Gly93Asp, p.Arg95Gln, p.Val97Met) could not detectably
391 restore yeast growth, confirming their loss of function (Fig. 4B). The higher protein instability caused by
392 the substitutions of the β-hairpin residues was also apparent in yeast except for the p.Glu34Lys allele,
393 which, although highly unstable in HeLa cells, was stably expressed in yeast (Fig. 4B). Additionally, the
394 p.Cys84Arg and p.Lys57Asn proteins were expressed at lower levels than WT. In contrast, the remaining
395 proteins (p.Arg37Pro and p.Cys38Arg) exhibited high instability, with minimal detectable expression.
396 Regarding the complementation of the yeast growth deficit, only the p.Phe33Ser and p.Glu34Lys were able
397 to fully restore the growth as efficiently as the hWT protein (Fig. 4C), while the p.Cys84Arg and
398 p.Lys57Asn could only do so partially.

399 We assessed the relationship between HINT1 protein expression and their ability to rescue the yeast growth
400 by calculating the Spearman's correlation coefficient between those two variables for the three variant
401 clusters (Fig. 4C). Only the modified proteins of the β-hairpin cluster showed a strong positive linear

402 correlation between the expression levels of the altered proteins and their ability to rescue the growth
403 phenotype in the yeast. Although the correlation was not significant, likely due to the small sample size,
404 this suggests that these amino acid substitutions do not detrimentally impact the HINT1 enzymatic activity.

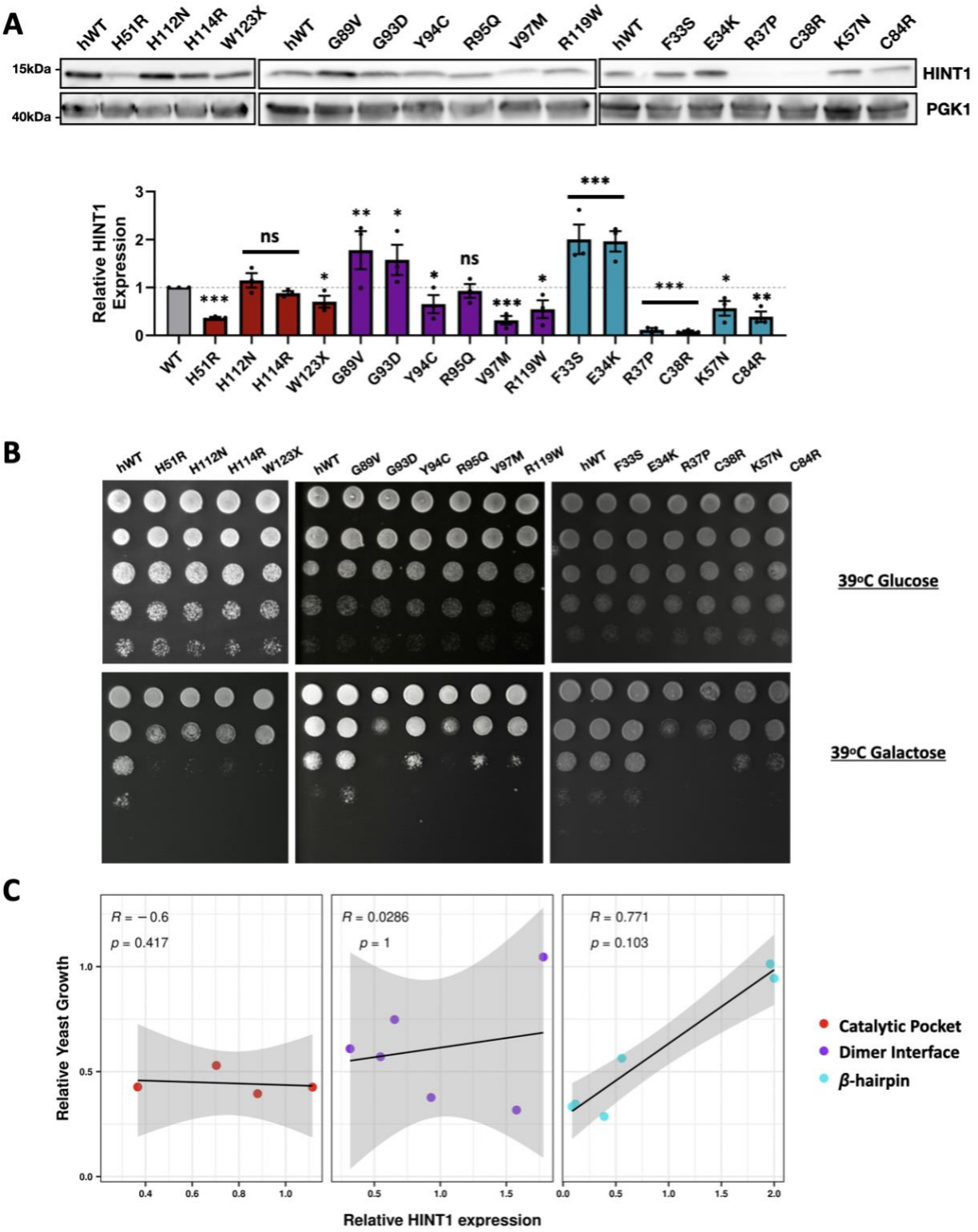

405

406 ***Figure 4 In vivo characterization of NMAN-causing variants.*** **A)** Immunoblotting analysis of total protein extracts

407 of a yeast HNT1-KO strain expressing the human mutant or WT HINT1 protein. Relative quantification of HINT1

408 levels was normalized to the expression of hWT protein. **B)** Genetic complementation analysis in a *HNT1*-deficient
409 yeast strain. A serial dilution of yeast culture was spotted in a plate and let grow for three days under permissive (2%
410 Glucose, 39ºC) and stress (2% Galactose, 39ºC) conditions. **C)** Linear coefficient correlations between the HINT1
411 protein expression and yeast growth relative to the hWT conditions. The correlations are calculated cluster-wise and
412 Spearman's correlation coefficients and corresponding p-values are indicated for each cluster.

413

414

415 **DISCUSSION**

416 The continuous effort to discover disease-causing genes is crucial for improving diagnostic accuracy, as
417 well as for advancing therapy development, since understanding the genetic basis enables the identification
418 of novel drug targets and facilitates precision medicine efforts. Next-generation sequencing (NGS)
419 technologies have dramatically increased the discovery of novel variants likely causing genetic diseases;
420 however, this larger number of identified variants (mostly missense) brings along the challenge of clinically
421 interpreting their pathogenicity. Strategies to infer variant causality include co-segregation with disease
422 phenotype, identification of additional affected families carrying the same variant, low allele frequency in
423 controls, computational predictions suggestive of pathogenicity, and *in vitro* and/or *in vivo* experimental
424 evidence supporting pathogenicity [1, 3, 56]. Variant interpretation, especially in ultra-rare disorders, relies
425 on robust computational and functional characterization strategies.

426 In this study, we used NMAN as an exemplary ultra-rare disease where the causal relationship with HINT1
427 is well-established and variant interpretation is facilitated by the presence of the clinical hallmark of
428 neuromyotonia. Nearly 30 variants spread along the protein sequence are reported in patients with
429 peripheral neuropathy, yet functional data are available for only approximately one-fourth of them.
430 Strikingly, approximately 40% of the *HINT1* variants reported in the ClinVar database have a germline
431 classification of uncertain significance, highlighting the need for re-assessment of their clinical
432 significance. Among the criteria given in the guidelines for variant interpretation by ACMG guidelines[57],
433 one of the most widely applicable parameters is *in silico* pathogenicity prediction. Many *in silico* tools exist

434 using different algorithms for evaluating variant impact; however, achieving concordance among them is
435 an increasing challenge[58]. We used three main *in silico* meta-predictors to assess the pathogenicity of
436 multiple missense variants in *HINT1* (CADD, REVEL, and AlphaMissense) and often also observed
437 conflicting interpretations (see Table 1). Among other factors, the function of proteins relies on their intact
438 native 3D conformation. However, none of the available pathogenicity predictors considers the quaternary
439 structure of the proteins [59]. This is especially important for HINT1 since its physiologically active state
440 in the cell is as a homodimer. Therefore, we additionally calculated the effect of the variants on the
441 monomer and dimer stability (folding free energies) using six different algorithms (Fig. 2) and the change
442 of solvent accessibility area upon homodimer formation (Additional File 3). Taken together, these analyses
443 allowed us to infer the contribution of each residue on dimer formation and how it was impacted by the
444 amino acid substitution.

445 Based on our combined approach, we could classify the HINT1 variants into four different groups: *1)*
446 truncation variants that lead to lack of HINT1 expression (i.e., p.Ser61Ter), *2)* variants that render a
447 dysfunctional catalytic pocket (i.e., p.His112Asn), *3)* variants that impact the dimer interface (i.e.
448 p.Gly93Asp), and *4)* variants that affect the distal β-hairpin and nearby loop (i.e. p.Arg37Pro). From a
449 functional perspective, overlaps exist between the variants of the dimer interface and the catalytic pocket.
450 Since HINT1 enzymatic cleft is formed by the two monomers, it is not surprising that residues of the
451 catalytic pocket (p.His114 and p.Trp123) are involved in maintaining the structure of the dimer or
452 alternatively, variants destabilizing the dimeric HINT1 form (p.Gly93Asp) completely abolish the
453 enzymatic activity. Notably, variants targeting residues located in the β-hairpin appear to have the most
454 significant destabilizing effect. However, this destabilization effect was not as pronounced in the yeast
455 allowing us to test the functionality of mutant proteins that are otherwise degraded (Fig. 4). Importantly,
456 we showed that they are unstable but enzymatically active, and their activity correlates with the HINT1
457 expression levels. Similarly, previous *in vitro* studies showed that the p.Cys84Arg allele mildly affected

458 the HINT1 3D structure and stability but retained its enzymatic activity despite being degraded in patient-
459 derived cells[7, 60].

460 Our characterization of each of the NMAN-associated proteins *in cellulo* and *in vivo* provided with
461 functional evidence of pathogenicity for additional seven variants classified as likely pathogenic
462 (p.Cys38Arg, p.Lys57Asn, p.Tyr94Cys, p.Val97Met, p.His114Arg, p.Arg119Trp) or VUS (p.Glu34Lys)
463 by the ACMG guidelines. Moreover, the functional assays demonstrated the deleterious character of the
464 variants where the *in silico* pathogenicity predictors showed contradictory results (i.e., p.Glu34Lys).
465 Studying the effect of the HINT1 missense variants on the protein function also allowed us to gain
466 mechanistic insights into NMAN pathomechanism. For instance, most missense variants led to the
467 expression of an unstable protein in patients, effectively leading to loss of protein function. Notably, HINT1
468 is a versatile protein with different properties within the cell, and it is unclear which of the activities is
469 associated with NMAN. The functional characterization we performed suggests that the enzymatic activity
470 of HINT1 is essential in the disease process. For example, the p.His112Asn allele results in a stable but
471 enzymatically inactive protein, and therefore, it is unable to rescue the growth deficiency in *HNT1*-KO
472 yeast. However, this altered protein has been demonstrated to still function as a transcriptional regulator of
473 the p53 tumor suppressor gene in cancerous cells. In addition, two substitutions (p.Phe33Ser and
474 p.Gly89Val) showed comparable functionality to the hWT protein in all our assays. Despite appearing
475 benign in these tests, both genetic and clinical evidence strongly support their pathogenic nature [7]. In fact,
476 *in vitro,* these substitutions have been shown to disrupt HINT1 SUMOylase activity [14] and their binding
477 with several interacting partners, such as calmodulin or the mu-opioid receptor, among others [61]. These
478 variants are, therefore, of particular interest in further uncovering both known and unknown HINT1
479 functions that might contribute to disease pathology.

480 Taken together, all NMAN-causal variants lead to a similar outcome, i.e., lack of a functional HINT1
481 enzyme in the cell. However, the establishment of four different classes of pathogenic variants based on
482 their structural and molecular characteristics suggests that a “one-size-fits-all" treatment would not apply

483 to all NMAN patients. The assay pipeline we developed can be used not only to assess the pathogenicity of
484 any new and uncharacterized variant in HINT1 but also serves as a tool to define the variant sub-class to
485 tailor the therapeutic strategy accordingly. For example, the NMAN-associated variants belonging to the β-
486 hairpin cluster preserve HINT1 enzymatic activity and show a linear correlation between HINT1 protein
487 expression and the rescue of yeast growth. Notably, most of the recurrent and high-frequency variants (e.g.,
488 p.Arg37Pro) belong to this cluster. Therefore, they seem to be ideal candidates for a pharmacochaperone
489 therapeutic approach. This approach involves a small molecule that could bind and stabilize the mutant
490 HINT1 protein *in vivo* and in this way restore its functionality. A similar strategy has been successfully
491 applied to treat cystic fibrosis, where a small molecule stabilizes the cystic fibrosis transmembrane
492 conductance regulator (CFTR) channel, reversing the effects of the pathogenic variant and slowing the
493 disease progression [62].

494 **CONCLUSIONS**

495 In summary, our standardized experimental pipeline allows for the characterization of newly discovered
496 HINT1 variants in the context of NMAN. Our work highlights the value of combining structural and
497 functional approaches to understand better the underlying disease mechanisms. Our findings provide the
498 rational basis for patient stratification and development of personalized treatment strategies.

499

500 **LIST OF ABBREVIATIONS**

501	ACMG	American College of Medical Genetics and Genomics
502	AF	Allele frequency
503	CADD	Combined Annotation Dependent Depletion
504	CH	Compound heterozygous
505	CMT	Charcot-Marie-Tooth disease
506	DMP	Dimethyl pimelimidat
507	FDA	U.S. Food and Drug Administration

gnomAD	Genome Aggregation Database
Hm	Homozygous
hWT	human HINT1 wild-type
kDA	kilodalton
KO	Knock-out
NGS	Next-generation sequencing
NMAN	Neuromyotonia-associated Axonal Neuropathy
PDB	Protein Data Bank
REVEL	Rare Exome Variant Ensemble Learner
VUS	Variant of Uncertain Significance

SUPPLEMENTARY INFORMATION

The following supplementary material is available:

Additional File 1: Overview of all HINT1 variants submitted to the ClinVar database.

Additional File 2: NMAN-associated missense variants mapped to the ungapped multiple sequence alignment of HINT1.

Additional File 3: Overview of the ΔΔG distributions calculated using different stability predictors and the solvent-accessible surface area.

DECLARATIONS

Ethics approval and consent to participate

Not applicable

Consent for publication

Not applicable

532 ***Availability of data and materials***

533 All data generated or analyzed during this study are included in this published article and its supplementary
534 information files

535 ***Competing interests***

536 The authors declare that they have no competing interests.

537 ***Funding***

538 This study was funded by The Research Foundation-Flanders (FWO): Research grants #G049217N and
539 #G0A2122N (to A.J.); postdoctoral fellowship to K.P. and A.C. (#12X8819N and #12AIV24N,
540 respectively). The AFM TELETHON: research grant to A.J (#23708) and trampoline grants to A.C., and
541 S.A.B. #24894, and #28730, respectively). The ABMM research grants to S.A.B., A.C., and A.J. . A.C. and
542 L.L.P.R. received funding from the European Union's Horizon 2020 research and innovation program
543 under the Marie Sklodowska-Curie grant agreement numbers 101108071 (Postdoctoral fellowship) and
544 101034290 (EMERALD International PhD Programme for Medical Doctors), respectively. T.L. is a
545 postdoctoral innovation mandate holder (HBC.2022.0194) of the Flanders Innovation & Entrepreneurship
546 Agency (VLAIO).

547 ***Authors' contributions***

548 SAB, TL, KP, SW, AJ: conception and design of the study; SAB, TL, AC, LLPR, KP, AJ, SW: acquisition
549 and analysis of the data; SAB, TL: data visualization; SAB, TL, AC, SW, AJ: drafting the text. All authors
550 read and approved the final manuscript.

551 ***Acknowledgements***

552 Not applicable

553

554

555 **REFERENCES**

556 1. Fernandez-Marmiesse A, Gouveia S, Couce ML: **NGS Technologies as a Turning Point in Rare Disease**
557 **Research , Diagnosis and Treatment**. *Curr Med Chem* 2018, **25**(3):404-432.

558 2. Danielsson K, Mun LJ, Lordemann A, Mao J, Lin CH: **Next-generation sequencing applied to rare**
559 **diseases genomics**. *Expert Rev Mol Diagn* 2014, **14**(4):469-487.

560 3. Boycott KM, Vanstone MR, Bulman DE, MacKenzie AE: **Rare-disease genetics in the era of next-**
561 **generation sequencing: discovery to translation**. *Nat Rev Genet* 2013, **14**(10):681-691.

562 4. **RARE Disease Facts. Global Genes** [https://globalgenes.org/rare-disease-facts/]

563 5. Tambuyzer E, Vandendriessche B, Austin CP, Brooks PJ, Larsson K, Miller Needleman KI, Valentine J,
564 Davies K, Groft SC, Preti R *et al*: **Therapies for rare diseases: therapeutic modalities, progress and**
565 **challenges ahead**. *Nat Rev Drug Discov* 2020, **19**(2):93-111.

566 6. Foksinska A, Crowder CM, Crouse AB, Henrikson J, Byrd WE, Rosenblatt G, Patton MJ, He K, Tran-
567 Nguyen TK, Zheng M *et al*: **The precision medicine process for treating rare disease using the artificial**
568 **intelligence tool mediKanren**. *Front Artif Intell* 2022, **5**:910216.

569 7. Zimon M, Baets J, Almeida-Souza L, De Vriendt E, Nikodinovic J, Parman Y, Battaloglu E, Matur Z,
570 Guergueltcheva V, Tournev I *et al*: **Loss-of-function mutations in HINT1 cause axonal neuropathy with**
571 **neuromyotonia**. *Nat Genet* 2012, **44**(10):1080-1083.

572 8. Peeters K, Chamova T, Tournev I, Jordanova A: **Axonal neuropathy with neuromyotonia: there is a**
573 **HINT**. *Brain* 2017, **140**(4):868-877.

574 9. Lassuthova P, Brozkova DS, Krutova M, Neupauerova J, Haberlova J, Mazanec R, Dvorackova N,
575 Goldenberg Z, Seeman P: **Mutations in HINT1 are one of the most frequent causes of hereditary**
576 **neuropathy among Czech patients and neuromyotonia is rather an underdiagnosed symptom**.
577 *Neurogenetics* 2015, **16**(1):43-54.

578 10. Zimon M, Battaloglu E, Parman Y, Erdem S, Baets J, De Vriendt E, Atkinson D, Almeida-Souza L,
579 Deconinck T, Ozes B *et al*: **Unraveling the genetic landscape of autosomal recessive Charcot-Marie-**
580 **Tooth neuropathies using a homozygosity mapping approach**. *Neurogenetics* 2015, **16**(1):33-42.

581 11. Bieganowski P, Garrison PN, Hodawadekar SC, Faye G, Barnes LD, Brenner C: **Adenosine**
582 **monophosphoramidase activity of Hint and Hnt1 supports function of Kin28, Ccl1, and Tfb3**. *J Biol*
583 *Chem* 2002, **277**(13):10852-10860.

584 12. Shah R, Maize KM, Zhou X, Finzel BC, Wagner CR: **Caught before Released: Structural Mapping of the**
585 **Reaction Trajectory for the Sofosbuvir Activating Enzyme, Human Histidine Triad Nucleotide**
586 **Binding Protein 1 (hHint1)**. *Biochemistry-Us* 2017, **56**(28):3559-3570.

587 13. Zhou X, Chou TF, Aubol BE, Park CJ, Wolfenden R, Adams J, Wagner CR: **Kinetic mechanism of human**
588 **histidine triad nucleotide binding protein 1**. *Biochemistry-Us* 2013, **52**(20):3588-3600.

589 14. Cortes-Montero E, Rodriguez-Munoz M, Sanchez-Blazquez P, Garzon J: **The Axonal Motor Neuropathy-**
590 **Related HINT1 Protein Is a Zinc- and Calmodulin-Regulated Cysteine SUMO Protease**. *Antioxid Redox*
591 *Signal* 2019, **31**(7):503-520.

592 15. Duan DD, Xie H, Shi HF, Huang WW, Ding F, Hong JK, Fan JS, Hu SY, Wang QW, Zhou MQ: **Hint1**
593 **Overexpression Inhibits the Cell Cycle and Induces Cell Apoptosis in Human Osteosarcoma Cells**.
594 *Onco Targets Ther* 2020, **13**:8223-8232.

595 16. Weiske J, Huber O: **The histidine triad protein Hint1 triggers apoptosis independent of its enzymatic**
596 **activity**. *J Biol Chem* 2006, **281**(37):27356-27366.

597 17. Wu XS, Bao TH, Ke Y, Sun DY, Shi ZT, Tang HR, Wang L: **Hint1 suppresses migration and invasion of**
598 **hepatocellular carcinoma cells in vitro by modulating girdin activity**. *Tumour Biol* 2016, **37**(11):14711-
599 14719.

600 18. Genovese G, Ghosh P, Li H, Rettino A, Sioletic S, Cittadini A, Sgambato A: **The tumor suppressor HINT1**
601 **regulates MITF and beta-catenin transcriptional activity in melanoma cells**. *Cell Cycle* 2012,
602 **11**(11):2206-2215.

603 19. Zhang Y, Da Q, Cao S, Yan K, Shi Z, Miao Q, Li C, Hu L, Sun S, Wu W *et al*: **HINT1 (Histidine Triad**
604 **Nucleotide-Binding Protein 1) Attenuates Cardiac Hypertrophy Via Suppressing HOXA5 (Homeobox**
605 **A5) Expression**. *Circulation* 2021, **144**(8):638-654.

606 20. Rodriguez-Munoz M, Sanchez-Blazquez P, Herrero-Labrador R, Martinez-Murillo R, Merlos M, Vela JM,
607 Garzon J: **The sigma1 receptor engages the redox-regulated HINT1 protein to bring opioid analgesia**
608 **under NMDA receptor negative control**. *Antioxid Redox Signal* 2015, **22**(10):799-818.

609 21. Garzon J, Herrero-Labrador R, Rodriguez-Munoz M, Shah R, Vicente-Sanchez A, Wagner CR, Sanchez-
610 Blazquez P: **HINT1 protein: a new therapeutic target to enhance opioid antinociception and block**
611 **mechanical allodynia**. *Neuropharmacology* 2015, **89**:412-423.

612 22. Rodriguez-Munoz M, Cortes-Montero E, Pozo-Rodrigalvarez A, Sanchez-Blazquez P, Garzon-Nino J: **The**
613 **ON:OFF switch, sigma1R-HINT1 protein, controls GPCR-NMDA receptor cross-regulation:**
614 **implications in neurological disorders**. *Oncotarget* 2015, **6**(34):35458-35477.

615 23. Rentzsch P, Witten D, Cooper GM, Shendure J, Kircher M: **CADD: predicting the deleteriousness of**
616 **variants throughout the human genome**. *Nucleic Acids Res* 2019, **47**(D1):D886-D894.

617 24. Ioannidis NM, Rothstein JH, Pejaver V, Middha S, McDonnell SK, Baheti S, Musolf A, Li Q, Holzinger E,
618 Karyadi D *et al*: **REVEL: An Ensemble Method for Predicting the Pathogenicity of Rare Missense**
619 **Variants**. *Am J Hum Genet* 2016, **99**(4):877-885.

620 25. Cheng J, Novati G, Pan J, Bycroft C, Zemgulyte A, Applebaum T, Pritzel A, Wong LH, Zielinski M, Sargeant
621 T *et al*: **Accurate proteome-wide missense variant effect prediction with AlphaMissense**. *Science* 2023,
622 **381**(6664):eadg7492.

623 26. Jaganathan K, Kyriazopoulou Panagiotopoulou S, McRae JF, Darbandi SF, Knowles D, Li YI, Kosmicki JA,
624 Arbelaez J, Cui W, Schwartz GB *et al*: **Predicting Splicing from Primary Sequence with Deep Learning**.
625 *Cell* 2019, **176**(3):535-548 e524.

626 27. Schymkowitz J, Borg J, Stricher F, Nys R, Rousseau F, Serrano L: **The FoldX web server: an online force**
627 **field**. *Nucleic Acids Res* 2005, **33**(Web Server issue):W382-388.

628 28. Worth CL, Preissner R, Blundell TL: **SDM--a server for predicting effects of mutations on protein**
629 **stability and malfunction**. *Nucleic Acids Res* 2011, **39**(Web Server issue):W215-222.

630 29. Pires DE, Ascher DB, Blundell TL: **mCSM: predicting the effects of mutations in proteins using graph-**
631 **based signatures**. *Bioinformatics* 2014, **30**(3):335-342.

632 30. Pires DE, Ascher DB, Blundell TL: **DUET: a server for predicting effects of mutations on protein**
633 **stability using an integrated computational approach**. *Nucleic Acids Res* 2014, **42**(Web Server
634 issue):W314-319.

635 31. Frappier V, Chartier M, Najmanovich RJ: **ENCoM server: exploring protein conformational space and**
636 **the effect of mutations on protein function and stability**. *Nucleic Acids Res* 2015, **43**(W1):W395-400.

637 32. Rodrigues CH, Pires DE, Ascher DB: **DynaMut: predicting the impact of mutations on protein**
638 **conformation, flexibility and stability**. *Nucleic Acids Res* 2018, **46**(W1):W350-W355.

639 33. Janin J: **Principles of protein-protein recognition from structure to thermodynamics**. *Biochimie* 1995,
640 **77**(7-8):497-505.

641 34. Mitternacht S: **FreeSASA: An open source C library for solvent accessible surface area calculations**.
642 *F1000Res* 2016, **5**:189.

643 35. Amor-Barris S, Hoyer H, Brauteset LV, De Vriendt E, Strand L, Jordanova A, Braathen GJ, Peeters K:
644 **HINT1 neuropathy in Norway: clinical, genetic and functional profiling**. *Orphanet J Rare Dis* 2021,
645 **16**(1):116.

646 36. Gietz RD, Schiestl RH: **High-efficiency yeast transformation using the LiAc/SS carrier DNA/PEG**
647 **method**. *Nat Protoc* 2007, **2**(1):31-34.

648 37. Kara B, Gül S, Güneş AS, Mülayim S, Yeşil G: **A Novel Mutation of HINT1 Gene in an Adolescent**
649 **Female with Axonal Neuropathy and Neuromyotonia**. *Journal of Pediatric Neurology* 2021, **19**(03):180-
650 182.

651 38. Reddy MA, Narmada GB, Sundarachary NV: **HINT1-Associated Axonal Neuropathy with**
652 **Neuromyotonia**. *Neurol India* 2023, **71**(2):363-365.

653 39. Boaretto F, Cacciavillani M, Mostacciuolo ML, Spalletta A, Piscosquito G, Pareyson D, Vazza G, Briani C:
654 **Novel loss-of-function mutation of the HINT1 gene in a patient with distal motor axonal neuropathy**
655 **without neuromyotonia**. *Muscle Nerve* 2015, **52**(4):688-689.

656 40. Candayan A, Cakar A, Yunisova G, Ozdag Acarli AN, Atkinson D, Topaloglu P, Durmus H, Yapici Z,
657 Jordanova A, Parman Y *et al*: **Genetic Survey of Autosomal Recessive Peripheral Neuropathy Cases**
658 **Unravels High Genetic Heterogeneity in a Turkish Cohort**. *Neurol Genet* 2021, **7**(5):e621.

659 41. Shchagina OA, Milovidova TB, Murtazina AF, Rudenskaya GE, Nikitin SS, Dadali EL, Polyakov AV:
660 **HINT1 gene pathogenic variants: the most common cause of recessive hereditary motor and sensory**
661 **neuropathies in Russian patients**. *Mol Biol Rep* 2019.

662 42. Tessa A, Schifino M, Salvo E, Trovato R, Cesana L, Frosini S, Pasquariello R, Sgherri G, Battini R, Bonaglia
663 MC *et al*: **Small Complex Rearrangement in HINT1-Related Axonal Neuropathy**. *Genes (Basel)* 2024,
664 **15**(11).

665 43. Malcorps M, Amor-Barris S, Burnyte B, Vilimiene R, Armirola-Ricaurte C, Grigalioniene K, Ekshteyn A,
666 Morkuniene A, Vaitkevicius A, De Vriendt E *et al*: **HINT1 neuropathy in Lithuania: clinical, genetic, and**
667 **functional profiling**. *Orphanet J Rare Dis* 2022, **17**(1):374.

668 44. Schubach M, Maass T, Nazaretyan L, Roner S, Kircher M: **CADD v1.7: using protein language models,**
669 **regulatory CNNs and other nucleotide-level scores to improve genome-wide variant predictions**.
670 *Nucleic Acids Res* 2024, **52**(D1):D1143-D1154.

671 45. Tordai H, Torres O, Csepi M, Padanyi R, Lukacs GL, Hegedus T: **Analysis of AlphaMissense data in**
672 **different protein groups and structural context**. *Sci Data* 2024, **11**(1):495.

673 46. Meng L, Fu J, Lv H, Zhang W, Wang Z, Yuan Y: **Novel mutations in HINT1 gene cause autosomal**
674 **recessive axonal neuropathy with neuromyotonia in two cases of sensorimotor neuropathy and one**
675 **case of motor neuropathy**. *Neuromuscul Disord* 2018, **28**(8):646-651.

676 47. Rauchenzauner M, Fruhwirth M, Hecht M, Kofler M, Witsch-Baumgartner M, Fauth C: **A Novel Variant in**
677 **the HINT1 Gene in a Girl with Autosomal Recessive Axonal Neuropathy with Neuromyotonia:**
678 **Thorough Neurological Examination Gives the Clue**. *Neuropediatrics* 2016, **47**(2):119-122.

679 48. Rozevska M, Rots D, Gailite L, Linde R, Mironovs S, Timcenko M, Linovs V, Locmele D, Micule I, Lace
680 B *et al*: **The most common European HINT1 neuropathy variant phenotype and its case studies**. *Front*
681 *Neurol* 2023, **14**:1084335.

682 49. Lewis HS, Srinivasa Sekaran BS, Stefans V, Veerapandiyan A: **Clinical Reasoning: A 6-Year-Old Boy**
683 **With Muscle Twitching**. *Neurology* 2021, **96**(2):e301-e304.

684 50. Fang J, Huang H, Lei Q, Luo Y, Tang Z, Shi X, Tang JG: **Myasthenia gravis coexisting with HINT1-**
685 **related motor axonal neuropathy without neuromyotonia: a case report**. *BMC Neurol* 2022, **22**(1):168.

686 51. Lin S, Xu LQ, Xu GR, Guo LL, Lin BJ, Chen WJ, Wang N, Lin Y, He J: **Whole exome sequencing reveals**
687 **a broader variant spectrum of Charcot-Marie-Tooth disease type 2**. *Neurogenetics* 2019.

688 52. Morel V, Campana-Salort E, Boyer A, Esselin F, Walther-Louvier U, Querin G, Latour P, Lia AS,
689 Magdelaine C, Beze-Beyrie P *et al*: **HINT1 Neuropathy: expanding the genotype and phenotype**
690 **spectrum**. *Clin Genet* 2022.

691 53. Zhao H, Race V, Matthijs G, De Jonghe P, Robberecht W, Lambrechts D, Van Damme P: **Exome sequencing**
692 **reveals HINT1 mutations as a cause of distal hereditary motor neuropathy**. *Eur J Hum Genet* 2014,
693 **22**(6):847-850.

694 54. Xu J, Yang Y, Liu Y: **[Analysis of HINT1 gene variant in a case with neuromyotonia and axonal**
695 **neuropathy]**. *Zhonghua Yi Xue Yi Chuan Xue Za Zhi* 2019, **36**(8):817-820.

696 55. Xu L, Wang G, Lv X, Zhang D, Yan C, Lin P: **A novel mutation in HINT1 gene causes autosomal**
697 **recessive axonal neuropathy with neuromyotonia, effective treatment with carbamazepine and review**
698 **of the literature**. *Acta Neurol Belg* 2022, **122**(5):1305-1312.

699 56. Sunyaev SR: **Inferring causality and functional significance of human coding DNA variants**. *Hum Mol*
700 *Genet* 2012, **21**(R1):R10-17.

701 57. Richards S, Aziz N, Bale S, Bick D, Das S, Gastier-Foster J, Grody WW, Hegde M, Lyon E, Spector E *et al*:
702 **Standards and guidelines for the interpretation of sequence variants: a joint consensus**
703 **recommendation of the American College of Medical Genetics and Genomics and the Association for**
704 **Molecular Pathology**. *Genet Med* 2015, **17**(5):405-424.

705 58. Wilcox EH, Sarmady M, Wulf B, Wright MW, Rehm HL, Biesecker LG, Abou Tayoun AN: **Evaluating the**
706 **impact of in silico predictors on clinical variant classification**. *Genet Med* 2022, **24**(4):924-930.

707 59. Schmidt A, Roner S, Mai K, Klinkhammer H, Kircher M, Ludwig KU: **Predicting the pathogenicity of**
708 **missense variants using features derived from AlphaFold2**. *Bioinformatics* 2023, **39**(5).

709 60. Shah RM, Maize KM, West HT, Strom AM, Finzel BC, Wagner CR: **Structure and Functional**
710 **Characterization of Human Histidine Triad Nucleotide-Binding Protein 1 Mutations Associated with**
711 **Inherited Axonal Neuropathy with Neuromyotonia**. *J Mol Biol* 2018, **430**(17):2709-2721.

712 61. Cortes-Montero E, Rodriguez-Munoz M, Sanchez-Blazquez P, Garzon-Nino J: **Human HINT1 Mutant**
713 **Proteins that Cause Axonal Motor Neuropathy Exhibit Anomalous Interactions with Partner Proteins**.
714 *Mol Neurobiol* 2021.

715 62. Li H, Pesce E, Sheppard DN, Singh AK, Pedemonte N: **Therapeutic approaches to CFTR dysfunction:**
716 **From discovery to drug development**. *J Cyst Fibros* 2018, **17**(2S):S14-S21.

717

718

719